Adhesion of *Crithidia fasciculata* promotes a rapid change in developmental fate driven by cAMP signaling

Shane Denecke[1,§], Madeline F. Malfara[2,§], Kelly R. Hodges[2], Nikki A. Holmes[2], Andre R. Williams[2], Julia H. Gallagher-Teske[3,4], Julia M. Pascarella[3], Abigail M. Daniels[1], Geert Jan Sterk[5], Rob Leurs[5], Gordon Ruthel[1], Rachel Hoang[3], Megan L. Povelones[2,*], Michael Povelones[1,*]

[1]Department of Pathobiology, School of Veterinary Medicine, University of Pennsylvania, Philadelphia, PA 19104, USA

[2]Department of Biology, Villanova University, Villanova, PA 19085, USA

[3]Department of Biology, Haverford College, Haverford, PA 19041, USA

[4]Cancer Clinical Trials Office, Department of Urology, Stanford University, Palo Alto, CA 94304, USA

[5]Amsterdam Institute for Molecules, Medicines and Systems, Division of Medicinal Chemistry, Faculty of Science, Vrije Universiteit Amsterdam, De Boelelaan 1108, 1081 HZ, Amsterdam, The Netherlands

Running title: Adhesion promotes rapid developmental change

§ Authors contributed equally

* To whom correspondence should be addressed: Michael Povelones: Department of Pathobiology, School of Veterinary Medicine, University of Pennsylvania, Philadelphia, PA, 19104; Megan Povelones: Department of Biology, Villanova University, Villanova, PA, 19085

mpove@vet.upenn.edu; Tel (215) 898-4144

megan.povelones@villanova.edu; Tel (610) 519-4863

Keywords: *Crithidia fasciculata*, adhesion, cyclic AMP, signaling, differentiation, kinetoplastid

Abstract

Kinetoplastids are single-celled parasites responsible for human and animal disease. For the vast majority of kinetoplastids, colonization of an insect host is required for transmission. Stable attachment to insect tissues via the single flagellum coincides with differentiation and morphological changes. Although this process is essential for the generation of infectious forms, the molecular mechanism driving differentiation following adherence is not well understood. To study this process, we elaborate upon an in vitro model in which flagellated swimming cells of the kinetoplastid *Crithidia fasciculata* rapidly differentiate following adhesion to artificial substrates. Manipulation of culture parameters revealed that growth phase and time had a strong influence on the proportion of adherent cells. Live imaging of cells transitioning from swimming to an attached cell fate show parasites undergoing a defined sequence of events including an initial adhesion near the base of the flagellum, immediately followed by flagellar shortening, cell rounding, and the formation of a hemidesmosome-like structure between the tip of the shortened flagellum and the substrate. We have also assayed the role of the cyclic AMP (cAMP) signaling pathway in differentiation of *C. fasciculata*. Pharmacological inhibition of cAMP phosphodiesterases eliminated the ability of swimming cells to attach without affecting their growth rate. Further, treatment with inhibitor did not affect the growth rate of established attached cells, indicating its effect is limited to a critical window of time during the early stages of adhesion. Finally, in swimming parasites we have shown that a receptor adenylate cyclase localizes to the distal portion of the flagellum. In attached cells it is absent from the shortened flagellum and instead localizes to the cell body. Similarly, a putative phosphodiesterase, found along the length of the flagellum, also relocalizes to the cell body in attached parasites. These data suggest that in *C. fasciculata* cAMP signaling is required for adherence, that cAMP flux in the flagellum of swimming cells is spatially restricted, and that signaling domains may be reorganized during differentiation and attachment. These studies contribute to our understanding of the flagellum as a multi-functional organelle integrating processes related to motility, signaling, attachment, and differentiation and further develop *C. fasciculata* as a model kinetoplastid.

Author Summary

Parasites from the order Kinetoplastida are transmitted by insects and cause diseases such as Leishmaniasis, Chagas disease, and Human African Trypanosomiasis. A key aspect of the life cycle of these parasites is their ability to adhere to surfaces within the insect and subsequently differentiate into forms that are transmissable to their next host. Here, we explore the molecular mechanisms underpinning both adherence and differentiation using the mosquito parasite *Crithidia fasciculata*. This organism is closely related to pathogenic species but grows to high densities in culture and adheres robustly in vitro. We identified factors affecting the rate of adherence and defined morphological stages of this process including rapid shortening of the cell's single flagellum. Using electron microscopy, we confirmed that adhesion to artificial substrates results in the formation of a filament-rich adhesive plaque at the tip of the flagellum that resembles the attachment to insect tissue. We also demonstrate the key role played by the cyclic AMP signaling pathway during adherence and differentiation. Specifically, pharmacological inhibition of enzymes that degrade cyclic AMP completely blocks adherence, and tagging of several proteins in this pathway show that their localization along the flagellum changes following differentiation to the attached form. These data provide insights into processes critical for all kinetoplastid life cycles.

61 ## Introduction

62 Organisms from the protozoan order Kinetoplastida impose a significant disease burden especially in low-income
63 countries [1]. *Trypanosoma brucei*, *Trypanosoma cruzi*, and *Leishmania* spp. are the etiological agents for
64 African trypanosomiasis, Chagas disease, and Leishmaniasis, respectively. These parasites also cause important
65 veterinary diseases, while still others impact insects critical for pollination. A deeper understanding of the biology
66 of these organisms can provide the basis for rational interventions to limit disease burden. Additionally,
67 kinetoplastid parasites are a compelling model for basic research, representing early-branching eukaryotes that are
68 divergent from more well-studied organisms such as insects, worms, and vertebrates.

69 Kinetoplastids primarily parasitize insects with only a handful of species using insects as a vector to infect other
70 organisms. In insects, kinetoplastids spend part of their life cycle adhered to the apical surface of an epithelial
71 lining. Adherence, also referred to as adhesion or attachment in the literature, often precedes a developmental
72 transition with distinct morphological and molecular changes. For example, in the kissing bug *Rhodnius prolixus*,
73 *T. cruzi* parasites bind to the perimicrovillar membrane in the posterior midgut, followed by the cuticular lining of
74 the hindgut, before being excreted by the insect as infectious metacyclics [2, 3]. Adherence is necessary not only
75 to maintain the parasites in the gut of their host, but to trigger differentiation to the infectious form. Similarly, *T.*
76 *brucei* adheres to salivary gland epithelium and *Leishmania* spp. adhere to the midgut and the stomodeal valve. In
77 each case, adherence precedes or is concurrent with differentiation to the final developmental form in the insect.
78 Despite the importance of adherence in the kinetoplastid insect life cycle, the relative inaccessibility of these
79 parasite stages in the insect, and the lack of a robust in vitro model to generate them, means that little is known
80 about adherence mechanisms and the signal transduction pathways that may connect adherence to developmental
81 progression.

82 *Crithidia fasciculata* is a monoxenous parasite of mosquitoes that developmentally transitions from a swimming
83 (nectomonad) cell with a long flagellum to an attached (haptomonad) cell with a dramatically shortened
84 flagellum. The tip of this flagellum is attached to the chitinous lining of the hindgut epithelium via a
85 hemidesmosome-like adhesive plaque. A morphologically similar plaque is found in the adhered forms of other
86 kinetoplastid species [4]. Remarkably, for *C. fasciculata* this developmental switch from a swimming to an
87 attached cell is readily produced in vitro by adhesion to a variety of substrates, including Millipore filters [5],

88 culture debris [6], and plastic dishes [7, 8]. Taking advantage of the ability to produce large numbers of
89 swimming and attached cells in culture, our recent transcriptomic analysis identified genes encoding putative
90 cyclic AMP (cAMP) signaling components that were differentially regulated in the different forms of *C.*
91 *fasciculata*. This led to the hypothesis that cAMP signaling may be involved in cell fate transitions in these
92 organisms [7].

93 Despite its importance, much remains unknown about cAMP signaling in kinetoplastids [9]. The cAMP second
94 messenger is created from ATP by adenylate cyclases (ACs), many of which are transmembrane receptor
95 adenylate cyclases (RACs) that probably act as receptors for unidentified ligands. The RAC family of ACs is
96 dramatically expanded in *T. brucei*, in which they localize to the flagellum, either along the length or at the distal
97 tip [10]. In many systems protein kinase A (PKA) acts downstream of cAMP, but in kinetoplastids, [11, 12], PKA
98 is independent cAMP [13]. Instead, several cAMP response proteins (CARPs) are thought to mediate
99 downstream events. Phosphodiesterases (PDEs) terminate the signal by degrading cAMP to 5'-AMP. In *T. brucei*,
100 some of these PDEs are localized to the flagellum, while others are found in the cell body [14]. It has been
101 proposed that PDEs act to limit the diffusion of cAMP and create spatially restricted signaling microdomains [15].
102 This paradigm has also been demonstrated in other eukaryotic systems [16].

103 Using a robust and quantitative adherence assay and imaging of live and fixed cells, we have defined the process
104 of adherence and the conditions that promote it in vitro. In addition, we have used pharmacological inhibitors to
105 probe the role of cAMP signaling during the transition to an attached state. Finally, we show the localization of
106 putative components of the *C. fasciculata* cAMP signaling pathway to the flagellum in swimming cells and show
107 striking changes in the distribution of these proteins upon flagellar shortening. These findings support the use of
108 *C. fasciculata* as a model to understand the spatial regulation of signal transduction in the context of adherence
109 and differentiation of kinetoplastid parasites.

110

111 **Results**

112

113 Culture conditions impact in vitro adherence of *C. fasciculata*

114 To probe the mechanism of *C. fasciculata* adherence, we used an in vitro assay to determine which conditions
115 impact the adherence rate. Swimming cells, grown on a shaker, were transferred to fresh culture plates and
116 incubated without shaking to allow cells to adhere. Plates were washed to remove non-adherent cells and then the
117 number of single adhered cells in representative fields were quantitated (Fig 1A). Over the next 24 hours, these
118 single cells divide to form attached rosettes. Cells in a rosette can undergo division to produce either two attached
119 cells or two swimming cells that can leave the rosette. Some proportion of these newly-produced swimming cells
120 can also encounter the dish and become attached. In our standard assay, swimming cells were again washed away
121 at 24 hours and rosettes with four or more cells in representative fields were quantitated.

122 By varying the length of plating time prior to washing, we found that the length of this incubation step was
123 directly proportional to the number of attached parasites, with the longest time we tested, 240 minutes, producing
124 the greatest number of rosettes (Fig 1 B,C). Consistent with a previous report [17], we also found that the growth
125 phase of the cultured cells had a strong effect on the rate of adherence. Cells from an early log phase culture (10^7
126 cells/mL) adhered and differentiated at a higher frequency compared with the same number of cells taken from a
127 stationary phase culture (10^8 cells/mL; Fig 1D). In addition to having a reduced rate of cell division, stationary
128 phase cells are morphologically distinct from cells in exponentially growing cultures, with the latter being rounder
129 and shorter (Figure S1). Increasing the total number of cells used in the adherence assay, provided those cells
130 were taken from a culture in log-phase, proportionally increased the total number of attached cells but had
131 relatively little impact on the percentage of cells that adhered during the 2 hour incubation (Fig 1E). These data
132 suggest that in vitro adherence of *C. fasciculata* happens at a constant rate and is inversely correlated with the
133 culture density before the assay begins but not while adherence occurs.

134

135 ## Mechanism of attachment of *C. fasciculata* in vitro

136 To examine the stages of adherence and differentiation of *C. fasciculata* more precisely, we used time-lapse
137 microscopy to follow parasites in environmentally controlled conditions. Using flagellar shortening and cell
138 rounding as morphological markers for differentiation, we observed that these events were always preceded by an
139 initial adhesion event (Videos S1,S2). During this event, cells first adhere to the plate via their anterior end, near

140 the flagellar pocket, and then begin to retract their flagellum. As this happens, the cells become rounder as they
141 undergo their first cellular division as adherent cells. In certain cases, cell division occurs prior to the full
142 retraction of the flagellum, but this was rare. Parasites sometimes adhered in pairs, a phenomenon that has been
143 reported previously [18]. In this case, one cell of the pair will typically detach and swim away (Video S2). From
144 these experiments, it was also possible to directly measure the rate of flagellar shortening, revealing that the
145 flagellum retracts at a relatively constant rate until it is no longer visible at around 2 hours (Fig 2).

146 While parasites initially adhere near the base of their flagellum, stably attached cells are connected to the substrate
147 via the distal tip of the shortened flagellum. Previous reports on *C. fasciculata* and other kinetoplastids have
148 described plaques at the site of attachment that ultrastructurally resemble hemidesmosomes [6]. Since most
149 imaging of the adhesive structure was performed on parasites adhered to the insect, we used transmission electron
150 microscopy (TEM) to determine if hemidesmosomes were present in attached cells where they contact the culture
151 plate. Consistent with prior findings [8], a cross-section of rosettes showed an osmophilic, filamentous plaque at
152 the distal tip of the shortened flagellum adjacent to the substrate (Fig 3 A-B). When we detached adherent cells
153 from culture plates by scraping prior to fixation, the hemidesmosome appeared intact, indicating that attachment
154 mediated by this structure can be physically disrupted (Fig 3C). Fibrous, desmosome-like structures appear to
155 connect the proximal part of the flagellum to the cell body at the flagellar pocket, features which have also been
156 noted in prior studies and which are probably components of the flagellar attachment zone (FAZ) (Fig 3A-C) [6,
157 19, 20]. When cells were sectioned *en face* near the attachment site with the culture plate, we observed that the
158 distal portion of the flagellum containing the hemidesmosome was somewhat enlarged and extended beyond the
159 termination point of flagellar axoneme (Fig 3D). In these sections, hemidesmosomes are circular and the degree to
160 which they are stained by uranyl acetate is likely a function of how close to the culture plate they were sectioned
161 (Fig 3D,E). By contrast, in swimming cells, we only found FAZ-like structures connecting the flagellum to the
162 pocket but did not observe hemidesmosomes at the distal end of the flagellum (Fig 3F). A notable feature of both
163 attached cells and scraped attached cells was an extracellular network of filamentous material attached to the
164 plasma membrane of the cell body (Fig 3G and 3A-D). In swimming cells, similar material was sometimes
165 observed in the flagellar pocket itself, but not on the cell surface (Fig 3F).

166

167 Pharmacological Inhibition of PDEs blocks adherence without affecting growth

168 Our prior work showed that cAMP signaling components are upregulated in swimming *C. fasciculata* relative to
169 attached parasites [7]. To test whether manipulating the cAMP pathway could influence the ability of *C.*
170 *fasciculata* to adhere to plastic in vitro, we used previously validated compounds that are known to inhibit cAMP
171 PDEs in the related parasite, *T. brucei* [21]. As PDEs terminate the signal by degrading the cAMP second
172 messenger, inhibition of these enzymes has been shown to increase the amount of cAMP in the parasite [22]. The
173 first compound we tested is known as NPD-001 or Compound A (CpdA) (hereafter NPD-001). The addition of 10
174 μM of NPD-001 to the adherence assay completely blocked parasite attachment to the plate, resulting in no single
175 adhered cells after 2 hours of incubation and no visible rosettes after 24 hours of growth (Fig 4A). Interestingly, a
176 related compound, NPD-008, had only a minor effect on adhesion, slightly reducing the number of single adhered
177 cells after 2 hours of incubation (Fig 4A). To determine if the effect of NPD-001 on attachment was dose-
178 dependent, we performed an adherence assay with both 1 μM and 0.1 μM of the compound. Although the effect
179 of 1 μM was comparable to that of 10 μM, 0.1 μM had a moderate effect on adhesion, suggesting a dose response.
180 The same concentrations of a related compound, NPD-226, also significantly reduced the number of adhered cells
181 both at 2 hours and at 24 hours at all three concentrations compared to vehicle-treated controls (Fig 4B). A fourth
182 compound, NPD-055, had a minor effect on adherence at the highest concentration (10 μM, Fig S3).

183 To confirm that the adherence-blocking activity of the PDE inhibitors was not due to cell toxicity, we measured
184 growth rates of swimming cultures of *C. fasciculata* (maintained on a shaker) in the presence of NPD-001.
185 Addition of this compound to the media did not affect the growth rate of swimming cells compared to vehicle- or
186 untreated control cells (Fig 5A). Furthermore, addition of NPD-001 to cells that were already differentiated to the
187 attached state did not affect their attachment or their doubling time over the course of 16 hours (Fig 5B). In this
188 experiment, we did observe new adherence of swimming cells produced from the rosettes in the vehicle-treated
189 control. Consistent with our previous finding (Fig 4A), although new swimming cells were produced from the
190 rosettes, in NPD-001 treated cultures, they failed to adhere.

191

192 cAMP signaling proteins are localized to the flagellum

193 In other kinetoplastids, components of cAMP signaling pathways are localized to flagellar subdomains, indicating
194 that this organelle may be involved in spatially restricting the distribution of this second messenger [10, 14]. To
195 see if this feature is also present in *C. fasciculata*, we localized a putative receptor adenylate cyclase (*Cf*RAC1)
196 and a putative cAMP phosphodiesterase (*Cf*PDEA) by fusing a GFP protein to the C-terminus of each open
197 reading frame and introducing these constructs into parasites as episomes (Fig S4). In swimming *C. fasciculata*,
198 *Cf*PDEA::GFP was found along the length of the flagellum, often appearing as two parallel lines of puncta (Fig
199 6). The extent of *Cf*PDEA::GFP is somewhat diminished along the portion of the flagellum in the flagellar pocket.
200 *Cf*RAC1::GFP was found in similar puncta, but was restricted to the distal third of the flagellum in swimming
201 parasites (Fig 6, Fig S5). We compared both of these localization patterns to another cell line in which a YFP
202 sequence was fused to one of the endogenous copies of the *Cf*PF16 gene (Fig S4), a component of the central pair
203 of the flagellar axoneme [23]. *Cf*PF16::YFP was uniformly distributed along the length of the flagellum in a
204 single continuous line without obvious puncta. No fluorescent signal was detected in parental CfC1 cells (Fig S6).

205 We then followed these localization patterns as cells transitioned from the swimming to the attached form. As
206 expected, *Cf*PF16::YFP could still be detected in the shortened flagellum which, as supported by our EM studies,
207 retains the central pair. However, *Cf*RAC1::GFP was no longer localized to the flagellum and was instead
208 distributed across the entire cell body. A similar redistribution was also observed in attached cells expressing
209 *Cf*PDEA::GFP (Fig 6). To compare expression levels of these proteins in attached and swimming *C. fasciculata*,
210 we performed western blotting using an anti-GFP antibody. Consistent with our microscopy results,
211 *Cf*PDEA::GFP and *Cf*RAC1::GFP are readily detected in both swimming and attached parasites despite their
212 different subcellular localizations (Fig 6). No fluorescent or anti-GFP western signal was observed in the parental
213 cells (Fig S6).

214

215 **Discussion**

216 Adherence and differentiation are both critical for the successful completion of kinetoplastid life cycles. While
217 signal transduction pathways driving differentiation have been described in multiple species, virtually nothing is
218 known about mechanisms of attachment and how this process is related to critical developmental events in the

219 insect vector. Numerous studies have found important roles for cAMP-based signaling in differentiation and
220 response to host environments, yet many questions remain unanswered in this area as well, including why
221 kinetoplastids have expanded their repertoire of RACs, what signals are sensed, and how downstream signals are
222 transduced. In addition, the significance of signaling subdomains in the flagellum is not understood. *C. fasciculata*
223 provides an opportunity to dissect the relationship between flagellar signaling and adherence in the context of
224 differentiation. We expect that, with some variations, this connection exists in all kinetoplastids. Our ability to
225 follow adherence and differentiation in live cells, coupled with a quantitative assay for adherence and expanding
226 tools for molecular genetics, opens a wide range of avenues for future exploration.

227 The mechanism of *C. fasciculata* attachment in vitro

228 The adherence of *C. fasciculata* and other kinetoplastids to substrates in vitro has been noted previously [6, 8, 17,
229 24-27]. Having developed a reproducible, quantitative assay for this phenomenon, we decided to explore factors
230 that would increase or decrease adherence. Consistent with previous work, we found that adherence of *C.*
231 *fasciculata* to artificial surfaces results in the formation of a hemidesmosome-like structure at the point of
232 attachment at the tip of the shortened flagellum. Due to the similarity of this attachment structure to that formed in
233 vivo [28, 29], we can use the in vitro system to determine the conditions required for its formation. As was
234 reported previously [17], we have also found that cultures in stationary phase are less likely to adhere compared to
235 log phase cultures, with a large drop off in adherence for parasites growing between 4 to $8x10^7$ cells/mL. *C.*
236 *fasciculata* parasites in stationary phase were shown to have a more elongated cell morphology compared to log
237 phase cells, and previous studies have demonstrated differential protein abundance between these cell states
238 possibly linked to their nutritional status [30]. Such nutrient deprivation has been shown to trigger adherence of *T.*
239 *cruzi* epimastigotes after which the parasites differentiate to the infectious metacyclic form [31]. In our assays,
240 this effect seems to result from an inherent difference between parasites in log- versus stationary-phase, as plates
241 seeded with large numbers of log phase cells can form nearly confluent layers, suggesting that there is no upper
242 limit to density in this assay. As adherence is linearly related to the number of plated log-phase cells, we also
243 conclude that it is not cooperative, and that each parasite adheres independently to the substrate. This is supported
244 by our TEM, live-cell, and fluorescence imaging studies which confirm that rosettes are formed by cell division of

245 individually adhered cells, which are each attached to the surface through their flagellum. In this case, the number
246 of attached parasites should be limited by substrate surface area. Consistently, previous studies on *Leishmania*
247 spp. have noted that scratching the surface, thereby increasing the available surface area, increases parasite
248 adherence [27], although this did not appear to trigger differentiation. It should be noted that the term "rosette"
249 has also been used to describe an observed tendency of some *Leishmania* spp. parasites to adhere to each other via
250 their flagella [32-35]. These rosettes are not adhered and are not formed through cell division, but instead result
251 from clustering of parasites. Thus far we have not seen this phenomenon in our *C. fasciculata* cultures.

252 We have also used this assay to probe the mechanism of adherence. *C. fasciculata* parasites initially contact the
253 dish via the anterior end of the cell body. We call this initial event "adhesion" which is rapidly followed by
254 flagellar shortening, cell rounding, and formation of the hemidesmosome. We call this fully differentiated state
255 "attached" reflecting the stable attachment between the tip of the flagellum and the substrate presumably
256 facilitated by the hemidesmosome-like structure and accompanied by changes in gene expression. In this study,
257 we have found that even at log phase the percentage of *C. fasciculata* parasites that stably attach to the dish is low
258 and increases linearly with time. Furthermore, our live-cell imaging studies show that not every cell that
259 encounters the plate undergoes differentiation to the attached form. These aborted adhesion events suggest that
260 only a subset of cells can make the transition at any one time, which may reflect stochastic variation, timing
261 within the cell cycle, or other factors. For example, it was shown previously that a subset of stationary-phase *C.*
262 *fasciculata* fail to agglutinate after treatment with peanut lectin, indicating possible variations in cell surface
263 molecules [30]. These glycoproteins and glycoconjugates may connect to the membrane by
264 glycosylphosphatidylinositol (GPI) anchors, which are found commonly among kinetoplastids. For example, it
265 has been suggested that differences in cell surface lipophosphoglycan (LPG) between promastigotes and
266 metacyclics in *L. major* may underpin the ability of the former to adhere to the midgut of their sandfly vector [36,
267 37]. These findings are particularly interesting in the context of the TEM data reported here, which show a lattice-
268 like filamentous molecule at the cell surface only in adherent cells. Similar material was detected in the flagellar
269 pocket of swimming cells, suggesting that it may be synthesized and secreted by this form, but not retained on the
270 surface. Determining the identity of this molecule will allow for exploration of possible roles in adhesion or
271 protection in the insect gut, as well as comparisons with other kinetoplastid species.

272 The predictable regularity of *C. fasciculata* attachment suggests a developmental program resulting in a distinct
273 cell state. Flagellar shortening occurs at a constant rate and seems triggered by the initial adhesion event. Our
274 TEM images show that the shortened flagellum of attached *C. fasciculata* are distinct from that of *Leishmania*
275 amastigotes in that the *C. fasciculata* axoneme retains the central pair of microtubules even at the tip. In addition
276 to the formation of hemidesmosome filaments, the *C. fasciculata* flagellar membrane at the point of attachment is
277 also expanded, as has been noted for haptomonads of other species [24, 26, 38]. From these data and our
278 experiments with NPD-001/CpdA, it appears that the final attached state, once established, is relatively stable. As
279 in other studies, we have found that the hemidesmosome is extremely resistant to detergents and enzymatic
280 digestion [39] but can be physically disrupted by scraping [40].

281 ## The role of cyclic AMP in *C. fasciculata* adhesion and differentiation

282 Strikingly, we found that inhibition of PDEs with NPD-001 completely blocked attachment. As treatment of
283 stably attached *C. fasciculata* parasites with NPD-001 did not cause the cells to detach nor did it prevent division
284 of attached cells, we hypothesize that elevated cAMP resulting from PDE inhibition disrupts the dynamic
285 transition from initial adhesion to stably attached. An alternative interpretation is that elevated cAMP impacts the
286 swimming cell population by dramatically reducing the subset of cells that are competent to adhere, meaning that
287 these cells would not even form initial adhesions. Our findings contribute to a large body of work showing that
288 signaling via the cAMP pathway plays a critical role in developmental transitions in kinetoplastid parasites [9,
289 41], including the epimastigote to metacyclic transition in *T. cruzi* [42] and the transitions to stumpy [42] and
290 procyclic form *T. brucei* [43]. However, in *T. brucei* there is evidence that differentiation may be triggered by
291 degradation products of cAMP, rather than cAMP itself [44]. In addition to differentiation, *T. brucei* requires
292 cAMP signaling for social motility, a process by which parasites generate and sense pH gradients and migrate
293 collectively through the tissues of their insect host, eventually attaching to the salivary gland epithelium and
294 differentiating to infectious metacyclics [12, 45, 46]. Treatment with CpdA/NPD-001 blocks social motility in
295 vitro [45], and genetic knockout of the *T. brucei* PDEB1 gene or other signaling components impairs or blocks
296 developmental progression through the fly [12, 46]. Due to the impact on social motility, the effect of these
297 manipulations on *T. brucei* attachment cannot be readily assessed.

298 Variations in flagellar length are a common feature of kinetoplastid life cycles [47], which may impact the
299 distribution of flagellar cAMP signaling proteins. We have found that GFP fusions of a putative RAC and PDE
300 (*Cf*RAC1::GFP and *Cf*PDEA::GFP) both localize to the flagellum in swimming *C. fasciculata*, with
301 *Cf*RAC1::GFP being enriched in the distal tip. Both *Cf*PDEA::GFP and *Cf*RAC1::GFP display punctate
302 localization patterns compared to *Cf*PF16::YFP. While *Cf*RAC1 has a predicted transmembrane domain, *Cf*PDEA
303 does not. However, in *T. brucei*, the phosphodiesterase TbPDEB1 is an integral component of the flagellum that is
304 resistant to detergent extraction [15]. Lipid analysis of the flagellar membrane has suggested lipid-raft like
305 membrane heterogeneity, which could also lead to uneven localization of our tagged proteins [48]. Therefore,
306 anchoring of *Cf*RAC1 and *Cf*PDEA to the flagellar membrane or structures within the flagellum could explain the
307 puncta that we observe. In addition, the parallel lines of signal found in both tagged cell lines is reminiscent of
308 intraflagellar transport trains, which associate with two sets of microtubule doublets on either side of the axoneme
309 [49]. The different distributions of these flagellar proteins, *Cf*RAC1 to the tip and *Cf*PDEA to the entire length, is
310 also consistent with observations in other organisms, in which specific amino acid sequences are required for
311 correct localization to flagellar subdomains [10]. However, how these domains are established and the
312 mechanisms for protein targeting are not yet clear.

313 Both tagged proteins are no longer enriched in the shortened flagellum of attached parasites, indicating
314 differential localization in the two developmental forms of *C. fasciculata*. As expected, *Cf*PF16::YFP was
315 retained in the shortened flagellum, as this structure still has its central pair of microtubules. It is unclear from
316 these studies if resident signaling proteins are relocalized from the flagellum to the cell body during transition
317 from swimming to attached, or whether newly synthesized signaling proteins in attached cells fail to enter the
318 flagellum, perhaps due to alterations in the machinery for flagellar protein sorting. Fluorescence time-course
319 imaging of differentiating cells should help reveal the dynamic localization patterns of cAMP signaling
320 components, which would convey critical information about this process.

321 Our data suggest that cAMP signaling acts during a relatively narrow window to facilitate the transition between
322 initial adhesion and stable attachment. As illustrated in Figure 7, our model is that the physical contact with the
323 surface during adhesion initiates flagellar shortening leading to local alterations in cAMP flux which then trigger

324 a developmental program including changes in transcript abundance and formation of the attachment plaque. This
325 would mean that the spatial restriction of RACs, PDEs, and other signaling proteins conveys important
326 statiotemporal information that is vital for successful developmental transitions. *C. fasciculata* is an attractive
327 system in which to tease out these processes, and future studies will explore the connection between flagellar
328 dynamics, signaling, adherence, and differentiation in this important group of parasites.

329

330 Materials and Methods

331 *Crithidia* maintenance

332 The Cf-C1 strain of *C. fasciculata* was used for all experiments in this study. This strain was originally obtained
333 from Dr. Stephen Beverley and was grown in complete medium (BHI) consisting of Brain Heart Infusion medium
334 (Sigma) supplemented with 20 µg/mL hemin (Sigma). Cells were maintained at 28 ºC in non-vented culture flasks
335 on a rocker and were maintained at a density between 10^5 and 10^8 cells/mL. Swimming cells were counted on a
336 hemocytometer following fixation in 0.3% formalin.

337 Plasmids and cell lines

338 The construct for C-terminal YFP tagging of the *C. fasciculata* putative axoneme central apparatus protein
339 CFAC1_170028000, named *Cf*PF16 for its shared homology to *L. mexicana* PF16 [23], was created using a
340 fusion PCR approach described previously [50]. The YFP and neomycin resistance genes were amplified from
341 pLENTv2eYFPNeo by PCR with forward primer pLENTeYFP_f and reverse primer pLENTNeo_r (Table 1). 500
342 bp of homology to the C-terminus of *Cf*PF16 was amplified from *C. fasciculata* genomic DNA using forward
343 primer PF16cterm500_f and reverse primer PF16cterm_r. 500 bp of homology to the 3' UTR of *Cf*PF16 was
344 amplified using PF16utr_f and PF16utr500_r. All three fragments were purified by PCR clean-up or gel
345 extraction and 20 ng of each fragment was combined in a fusion PCR reaction using PF16_500bpnest_f and
346 PF16_500bpnest_r. The resulting construct, PF16eYFPNeo, was gel extracted and ethanol precipitated. To create
347 a *C. fasciculata* CfPF16::YFP cell line, transfection was performed with 3.5 µg of PF16eYFPNeo introduced into
348 10^8 cells using a Human T-cell kit and IIb Nucleofector set to program X-001 (Lonza). Other transfections

349 described in this work used the same conditions except with *Tb*-BSF buffer (90 mM sodium phosphate, 5 mM
350 potassium chloride, 0.15 mM calcium chloride, 50 mM HEPES, pH 7.3) [51]. Immediately following transfection,
351 cells were transferred to 30 mL of BHI without selecting drug and diluted 10-fold. For each dilution, 1 mL was
352 plated into wells of a 24-well plate and cultured overnight without shaking. After approximately 18 hours of
353 recovery, 1 mL of BHI containing neomycin (G418) was added to each well, for a final selecting drug
354 concentration of 25 µg/mL. Resistant clones came up in 7-14 days and were fixed and screened for eYFP
355 fluorescence using wide-field microscopy. The resulting clonal cell line CfPF16YFP_A6 was used for these
356 studies and was validated by linking PCR across the gene with primer PF16ORF_f binding inside the gene and
357 reverse primer PF16UTR_r binding in the 3'UTR (outside of the area used for integration). To create the *C.*
358 *fasciculata Cf*RAC1::GFP and CfPDEA::GFP cell lines, the entire open reading frame of *Cf*RAC1
359 (CFAC1_090006500) or CfPDEA (CFAC1_140020300) were amplified from *C. fasciculata* genomic DNA and
360 cloned into the pNUSGFPcH vector [52] using NdeI and KpnI or NdeI and BglII restriction enzyme sites,
361 respectively. Following confirmation by sequencing (Eurofins Genomics), 10 µg of the final plasmid was
362 introduced into *C. fasciculata* as described above. Transfected cells were selected using BHI containing 80 µg/mL
363 hygromycin. After 7 days, selecting drug concentration was increased to 200 µg/mL and cells were screened by
364 fluorescence microscopy.

365 Adherence assay

366 Establishment of cultures of swimming and adherent *C. fasciculata* in vitro were adapted from our previous study
367 [7]. Briefly, cells from a rocking culture of swimmers were added to 60 mm non-treated tissue culture plates
368 (VWR) in 2 mL of BHI. For some experiments, cells were spun down in tubes at 800 rcf for 5 minutes and
369 resuspended in BHI. The cell suspension was allowed to sit in the 60 mm plates undisturbed at 28 ºC for the
370 indicated amounts of time during which adherence takes place (2 hours for the standard assay). Following this
371 incubation, each plate was washed 5 times with PBS before addition of fresh BHI media. When assays were
372 performed in 24-well plates, the same protocol was followed but the wash volume was 2 mL. Other assay
373 parameters were tested systematically and described in the results.

374 Quantitation of adherence was performed through imaging on a Zeiss Primovert Digital Microscope. Following
375 wash steps, plates were imaged by taking either 25 frames at 40x magnification or 10-25 frames at 20x
376 magnification. Freshly adhered cells (singlets) were counted either manually or, when large numbers of adhered
377 cells were present, by Fiji script [23]. Rosettes were counted manually as clusters of 4 or more cells at 24 hours.

378 Transmission electron microscopy and Giemsa staining

379 Swimming and attached *C. fasciculata* cells were processed and imaged using transmission electron microscopy
380 (TEM) performed in the Electron Microscopy Resource Lab (Perelman School of Medicine, University of
381 Pennsylvania). For swimming cells, 10^8 mid-log-phase cells were concentrated by centrifugation and resuspended
382 in TEM fix (0.1 M sodium cacodylate buffer, pH 7.4, containing 2.5% glutaraldehyde, and 2.0%
383 paraformaldehyde). For attached cells, rosette cultures in 60 mm dishes were established for 24 hours as described
384 above. 5 mL of TEM fix was added to the plate at room temperature. A second 24-hour attached sample was
385 generated by scraping cells off the plate with a disposable plastic scraper, concentrating by centrifugation, and
386 placing in TEM fix. All samples were fixed initially at room temperature for 2 hours and then placed at 4 ºC
387 overnight. After subsequent buffer washes, samples were post-fixed in 2.0% osmium tetroxide with 1.5%
388 $K_3Fe(CN)_6$ for 1 hour at room temperature and rinsed in water prior to *en bloc* staining with 2% uranyl acetate.
389 After dehydration through a graded ethanol series, the tissue was infiltrated and embedded in EMbed-812
390 (Electron Microscopy Sciences). Thin sections were stained with uranyl acetate and SATO lead and examined
391 with a JEOL 1010 electron microscope fitted with a Hamamatsu digital camera and AMT Advantage
392 NanoSprint500 software. Images of cells cut in cross section and *en face* were captured (Fig S2). Morphological
393 changes between mid-log phase and stationary phase cells were obtained by performing a cytologic cytocentrifuge
394 preparation and a standard Wright-Giemsa stain and imaging at 100x.

395 High content imaging

396 High content imaging was performed using an ImageXpress Micro 4-High Content imaging device (Molecular
397 Devices) at 40x and 60x using standard 24 (CellTreat) and black welled (Vision 4tituder) 24 well plates
398 respectively. To measure rosette growth, cells were allowed to adhere to standard plates for 2 hours followed by 5
399 washes with 2 mL of PBS and resuspension in fresh BHI media. Adhesion videos were obtained using black

400 welled plates by adding 4 x 10^5 cells to 500 µL of BHI media and allowing adhesion for 2 hours prior to imaging
401 at 1.25 min intervals.

402 Confocal microscopy and image processing

403 For fluorescence and confocal microscopy, 5 x 10^6 swimming cells from mid-log cultures were concentrated by
404 centrifugation at 800 rcf for 5 minutes, washed once in PBS, then resuspended in PBS at a final concentration of
405 10^7 cells/mL. 500 µL of this suspension was then pipetted onto coverslips pretreated with 0.01% poly-L-lysine.
406 After allowing cells to attach for 20 minutes at room temperature, coverslips were washed twice with PBS,
407 followed by fixation in 4% paraformaldehyde for 15 minutes. Coverslips were then washed again followed by
408 permeabilization with 0.1% Triton X-100 in PBS for 5 minutes. Coverslips were washed in PBS prior to staining
409 with 0.2 µg/mL DAPI in PBS for 5 minutes. After a final PBS wash, coverslips were mounted on a glass slide
410 using Vectashield mounting medium (Vector Laboratories). For fluorescence microscopy of attached cells, a
411 standard adherence assay was conducted, as described above, on 1.5 thickness glass-bottom dishes pre-coated
412 with poly-L-lysine (MatTek). After 24 hours of adherent growth, the final BHI wash contained 16%
413 formaldehyde added to a final concentration of 4%. The plate was processed from this point as described above
414 for the swimmer cell slides. The slides and plates were analyzed by confocal microscopy using a Leica SP5-II
415 with a 100x objective. A Z-series was acquired for GFP/YFP, DAPI and brightfield. Following image acquisition,
416 deconvolution analysis was performed on the fluorescent images using Huygens Essential deconvolution software
417 (version 17.04.1p2 64b; SVI). Brightfield images are single confocal sections with a flatfield correction applied.
418 All images of parental, *Cf*PDEA::GFP, and *Cf*RAC1::GFP were acquired with the same microscope settings.
419 Equivalent linear adjustments were made to the brightness of each image using Photoshop Version 23.5.1
420 (Adobe).

421 Western blot analysis

422 For swimming cultures, samples were generated from 2x10^6 log-phase cells. For adhered cultures, an equivalent
423 number of cells were grown on 60 mm dishes in stationary culture for 24 hours and then dislodged using a cell
424 scraper and counted by hemacytometer. Both swimming and dislodged adherent cells were transferred to
425 microcentrifuge tubes and collected by centrifugation, washed once with PBS, then resuspended in Laemmli

426 SDS-PAGE sample buffer at a concentration of $1x10^5$ cell equivalents/µl. Samples boiled for 5 min at 95 ºC and
427 centrifuged briefly. Cell equivalents of ~$1.5x10^6$ cells per lane were separated by 10% SDS-PAGE along with the
428 Precision Plus Protein Kaleidoscope standard (BioRad). The fractionated proteins were transferred to a PVDF
429 membrane. The membrane was then incubated in blocking buffer (PBS containing 5% milk and 0.2% Tween-20)
430 for 1 hour at room temperature. A mouse anti-GFP antibody (Roche) was used as the primary antibody at a 1:500
431 dilution in blocking buffer overnight at 4 °C. Horseradish peroxidase-conjugated goat anti-mouse IgG in blocking
432 buffer was used as the secondary antibody (1:5000). After washing, Enhanced Chemiluminescent Substrate
433 (BioRad) was used to develop the blots. For the loading control, the blot was reprobed with a rabbit anti-*Tb*BiP
434 antibody (a gift of Jay Bangs) at a 1:5000 dilution in blocking buffer, followed by washing and probing with an
435 anti-rabbit-HRP secondary antibody (1:5000). Images were taken by an Azure biosystems c600 using
436 chemiluminescence settings.

437 Pharmacological inhibition

438 Pharmacological inhibitors were dissolved in DMSO. For vehicle controls, an amount of DMSO equal to that of
439 the most concentrated sample was added. The compounds were described previously: NPD-001 [22], NPD-008
440 [53], NPD-055 [54], and NPD-226 [55].

441 Statistical analyses and data visualization

442 Prism Version 9.4.1 (458) (GraphPad Software) was used to generate all plots and for all statistical tests. Plots
443 were assembled into figures using Illustrator Version 26.5 (Adobe).

444

445 **Acknowledgments**

446 We thank Biao Zuo for preparing TEM samples and assistance with image acquisition and Koranda Walsh and
447 the PennVet Clinical Pathology lab for processing the Giemsa staining samples. We thank Emmanuel Tetaud,
448 Sam Dean, Eva Gluenz, and Tom Beneke for plasmids and advice. Thanks to Stephen Beverley for providing the
449 Cf-C1 wild-type *C. fasciculata* cell line and who, along with Wesley Warren, Chad Tomlinson, and Peter Myler,
450 made the unpublished genome sequence available on TriTrypDB. We thank Jay Bangs for providing the anti-BiP

451 antibody and Lindsay Bair, Laura Anastor-Walters, and Nancy Peltier for their technical assistance. We thank
452 Jesse Quatse for assistance with Photoshop. Finally, we acknowledge the PennVet Imaging Core for providing
453 access to instrumentation and analysis software used in live-cell and confocal imaging and image processing.

454

455 **References**

456

457 1. Diseases GBD, Injuries C. Global burden of 369 diseases and injuries in 204 countries and territories, 1990-
458 2019: a systematic analysis for the Global Burden of Disease Study 2019. Lancet. 2020;396(10258):1204-22. doi:
459 10.1016/S0140-6736(20)30925-9. PubMed PMID: 33069326; PubMed Central PMCID: PMCPMC7567026.

460 2. Goncalves CS, Avila AR, de Souza W, Motta MCM, Cavalcanti DP. Revisiting the *Trypanosoma cruzi*
461 metacyclogenesis: morphological and ultrastructural analyses during cell differentiation. Parasit Vectors.
462 2018;11(1):83. Epub 20180206. doi: 10.1186/s13071-018-2664-4. PubMed PMID: 29409544; PubMed Central
463 PMCID: PMCPMC5801705.

464 3. Kollien AH, Schaub GA. The development of *Trypanosoma cruzi* in triatominae. Parasitol Today.
465 2000;16(9):381-7. doi: 10.1016/s0169-4758(00)01724-5. PubMed PMID: 10951597.

466 4. Vickerman K, Tetley L. Flagellar surfaces of parasitic protozoa and their role in attachment. In: Bloodgood
467 RA, editor. Ciliary and Flagellar Membranes. Boston, MA: Springer US; 1990. p. 267-304.

468 5. Brooker BE. Flagellar Adhesion of *Crithidia fasciculata* to Millipore Filters. Protoplasma. 1971;72(1):19-25.

469 6. Brooker BE. Desmosomes and hemidesmosomes in the flagellate *Crithidia fasciculata*. Z Zellforsch Mikrosk
470 Anat. 1970;105(2):155-66. doi: 10.1007/BF00335467. PubMed PMID: 4195325.

471 7. Filosa JN, Berry CT, Ruthel G, Beverley SM, Warren WC, Tomlinson C, et al. Dramatic changes in gene
472 expression in different forms of *Crithidia fasciculata* reveal potential mechanisms for insect-specific adhesion in
473 kinetoplastid parasites. PLoS Negl Trop Dis. 2019;13(7):e0007570. Epub 2019/07/30. doi:
474 10.1371/journal.pntd.0007570. PubMed PMID: 31356610.

475 8. Hommel M, Robertson E. In vitro attachment of trypanosomes to plastic. Experientia. 1976;32(4):464-6. doi:
476 10.1007/BF01920798. PubMed PMID: 1269646.

477 9. Tagoe DN, Kalejaiye TD, de Koning HP. The ever unfolding story of cAMP signaling in trypanosomatids: vive
478 la difference! Front Pharmacol. 2015;6:185. Epub 20150907. doi: 10.3389/fphar.2015.00185. PubMed PMID:
479 26441645; PubMed Central PMCID: PMCPMC4561360.

480 10. Saada EA, Kabututu ZP, Lopez M, Shimogawa MM, Langousis G, Oberholzer M, et al. Insect stage-specific
481 receptor adenylate cyclases are localized to distinct subdomains of the *Trypanosoma brucei* flagellar membrane.
482 Eukaryot Cell. 2014;13(8):1064-76. Epub 20140530. doi: 10.1128/EC.00019-14. PubMed PMID: 24879126;
483 PubMed Central PMCID: PMCPMC4135804.

484 11. Gould MK, Bachmaier S, Ali JA, Alsford S, Tagoe DN, Munday JC, et al. Cyclic AMP effectors in African
485 trypanosomes revealed by genome-scale RNA interference library screening for resistance to the
486 phosphodiesterase inhibitor CpdA. Antimicrob Agents Chemother. 2013;57(10):4882-93. Epub 20130722. doi:
487 10.1128/AAC.00508-13. PubMed PMID: 23877697; PubMed Central PMCID: PMCPMC3811416.

488 12. Shaw S, Knüsel S, Abbühl D, Naguleswaran A, Etzensperger R, Benninger M, et al. Cyclic AMP signalling
489 and glucose metabolism mediate pH taxis by African trypanosomes. Nature Communications. 2022;13(1). doi:
490 10.1038/s41467-022-28293-w.

491 13. Bachmaier S, Volpato Santos Y, Kramer S, Githure GB, Klöckner T, Pepperl J, et al. Nucleoside analogue
492 activators of cyclic AMP-independent protein kinase A of *Trypanosoma*. Nature Communications. 2019;10(1).
493 doi: 10.1038/s41467-019-09338-z.

494 14. Oberholzer M, Marti G, Baresic M, Kunz S, Hemphill A, Seebeck T. The *Trypanosoma brucei* cAMP
495 phosphodiesterases TbrPDEB1 and TbrPDEB2: flagellar enzymes that are essential for parasite virulence. FASEB
496 J. 2007;21(3):720-31. Epub 20061213. doi: 10.1096/fj.06-6818com. PubMed PMID: 17167070.

497 15. Luginbuehl E, Ryter D, Schranz-Zumkehr J, Oberholzer M, Kunz S, Seebeck T. The N terminus of
498 phosphodiesterase TbrPDEB1 of *Trypanosoma brucei* contains the signal for integration into the flagellar
499 skeleton. Eukaryot Cell. 2010;9(10):1466-75. Epub 20100806. doi: 10.1128/EC.00112-10. PubMed PMID:
500 20693305; PubMed Central PMCID: PMCPMC2950416.

501 16. Baillie GS. Compartmentalized signalling: spatial regulation of cAMP by the action of compartmentalized
502 phosphodiesterases. FEBS Journal. 2009;276(7):1790-9. doi: 10.1111/j.1742-4658.2009.06926.x.

503 17. Scolaro EJ, Ames RP, Brittingham A. Growth-phase dependent substrate adhesion in *Crithidia fasciculata*. J
504 Eukaryot Microbiol. 2005;52(1):17-22. doi: 10.1111/j.1550-7408.2005.3315r.x. PubMed PMID: 15702975.

505 18. Hughes D, Simpson L, Schneider CA. Flagellar adherence of *Crithidia fasciculata* cells in culture. The
506 Journal of Protozoology. 1983;30(4):635-41. doi: 10.1111/j.1550-7408.1983.tb05335.x.

507 19. Sunter JD, Yanase R, Wang Z, Catta-Preta CMC, Moreira-Leite F, Myskova J, et al. *Leishmania* flagellum
508 attachment zone is critical for flagellar pocket shape, development in the sand fly, and pathogenicity in the host.
509 Proc Natl Acad Sci U S A. 2019;116(13):6351-60. Epub 20190308. doi: 10.1073/pnas.1812462116. PubMed
510 PMID: 30850532; PubMed Central PMCID: PMCPMC6442623.

511 20. Wheeler RJ, Sunter JD, Gull K. Flagellar pocket restructuring through the *Leishmania* life cycle involves a
512 discrete flagellum attachment zone. J Cell Sci. 2016;129(4):854-67. Epub 20160108. doi: 10.1242/jcs.183152.
513 PubMed PMID: 26746239; PubMed Central PMCID: PMCPMC4760377.

514 21. Veerman J, van den Bergh T, Orrling KM, Jansen C, Cos P, Maes L, et al. Synthesis and evaluation of analogs
515 of the phenylpyridazinone NPD-001 as potent trypanosomal TbrPDEB1 phosphodiesterase inhibitors and in vitro
516 trypanocidals. Bioorg Med Chem. 2016;24(7):1573-81. Epub 20160226. doi: 10.1016/j.bmc.2016.02.032.
517 PubMed PMID: 26935942.

518 22. de Koning HP, Gould MK, Sterk GJ, Tenor H, Kunz S, Luginbuehl E, et al. Pharmacological validation of
519 *Trypanosoma brucei* phosphodiesterases as novel drug targets. J Infect Dis. 2012;206(2):229-37. Epub 20120130.
520 doi: 10.1093/infdis/jir857. PubMed PMID: 22291195; PubMed Central PMCID: PMCPMC3379837.

521 23. Beneke T, Madden R, Makin L, Valli J, Sunter J, Gluenz E. A CRISPR Cas9 high-throughput genome editing
522 toolkit for kinetoplastids. R Soc Open Sci. 2017;4(5):170095. Epub 20170503. doi: 10.1098/rsos.170095.
523 PubMed PMID: 28573017; PubMed Central PMCID: PMCPMC5451818.

524 24. Beattie P, Gull K. Cytoskeletal architecture and components involved in the attachment of *Trypanosoma*
525 *congolense* epimastigotes. Parasitology. 1997;115 (Pt 1):47-55. doi: 10.1017/s0031182097001042. PubMed
526 PMID: 9280895.

527 25. Kleffmann T, Schmidt J, Schaub GA. Attachment of Trypanosoma cruzi epimastigotes to hydrophobic
528 substrates and use of this property to separate stages and promote metacyclogenesis. J Eukaryot Microbiol.
529 1998;45(5):548-55. doi: 10.1111/j.1550-7408.1998.tb05115.x. PubMed PMID: 9783457.

530 26. Skalický T, Dobáková E, Wheeler RJ, Tesařová M, Flegontov P, Jirsová D, et al. Extensive flagellar
531 remodeling during the complex life cycle of *Paratrypanosoma*, an early-branching trypanosomatid. Proceedings
532 of the National Academy of Sciences. 2017;114(44):11757-62. doi: 10.1073/pnas.1712311114.

533 27. Wakid MH, Bates PA. Flagellar attachment of Leishmania promastigotes to plastic film in vitro. Exp
534 Parasitol. 2004;106(3-4):173-8. doi: 10.1016/j.exppara.2004.03.001. PubMed PMID: 15172225.

535 28. Brooker BE. Flagellar attachment and detachment of *Crithidia fasciculata* to the gut wall of *Anopheles*
536 *gambiae*. Protoplasma. 1971;73(2):191-202. doi: 10.1007/BF01275594. PubMed PMID: 5126403.

537 29. Evans DA, Ellis DS, Stamford S. Ultrastructural studies of certain aspects of the development of
538 Trypanosoma congolense in Glossina morsitans morsitans. J Protozool. 1979;26(4):557-63. doi: 10.1111/j.1550-
539 7408.1979.tb04195.x. PubMed PMID: 544799.

540 30. Alcolea PJ, Alonso A, García-Tabares F, Toraño A, Larraga V. An insight into the proteome of *Crithidia*
541 *fasciculata* choanomastigotes as a comparative approach to axenic growth, peanut lectin agglutination and
542 differentiation of *Leishmania* spp. promastigotes. PloS one. 2014;9(12):e113837. doi:
543 10.1371/journal.pone.0113837.

544 31. Figueiredo RC, Rosa DS, Soares MJ. Differentiation of *Trypanosoma cruzi* epimastigotes: metacyclogenesis
545 and adhesion to substrate are triggered by nutritional stress. The Journal of parasitology. 2000;86(6):1213-8. doi:
546 10.1645/0022-3395(2000)086[1213:DOTCEM]2.0.CO;2. PubMed PMID: 11191893.

547 32. Greenblatt CL, Handman E, Mitchell GF, Battye FL, Schnur LF, Snary D. Phenotypic diversity of cloned
548 lines of Leishmania major promastigotes. Z Parasitenkd. 1985;71(2):141-57. doi: 10.1007/BF00926265. PubMed
549 PMID: 3922149.

550 33. Iovannisci DM, Plested CP, Moe GR. Evidence for rosettes as an unrecognized stage in the life cycle of
551 Leishmania parasites. J Eukaryot Microbiol. 2010;57(5):405-14. Epub 20100805. doi: 10.1111/j.1550-
552 7408.2010.00496.x. PubMed PMID: 20707828; PubMed Central PMCID: PMCPMC3086735.

553 34. Leishman WB. Critical Review: Kala Azar and Tropical Sore. QJM: An International Journal of Medicine.
554 1911;os5(1):109-52. doi: 10.1093/oxfordjournals.qjmed.a069298.

555 35. Noguchi H, Tilden EB. Comparative Studies of Herpetomonads and Leishmanias : I. Cultivation of
556 Herpetomonads from Insects and Plants. J Exp Med. 1926;44(3):307-25. doi: 10.1084/jem.44.3.307. PubMed
557 PMID: 19869186; PubMed Central PMCID: PMCPMC2131765.

558 36. Sacks D, Kamhawi S. Molecular aspects of parasite-vector and vector-host interactions in leishmaniasis. Annu
559 Rev Microbiol. 2001;55:453-83. doi: 10.1146/annurev.micro.55.1.453. PubMed PMID: 11544364.

560 37. Pimenta PF, Turco SJ, McConville MJ, Lawyer PG, Perkins PV, Sacks DL. Stage-specific adhesion of
561 *Leishmania* promastigotes to the sandfly midgut. Science. 1992;256(5065):1812-5. doi: 10.1126/science.1615326.
562 PubMed PMID: 1615326.

563 38. Warburg A, Hamada GS, Schlein Y, Shire D. Scanning electron microscopy of *Leishmania major* in
564 *Phlebotomus papatasi*. Z Parasitenkd. 1986;72(4):423-31. doi: 10.1007/BF00927886. PubMed PMID: 3751230.

565 39. Skalicky T, Dobakova E, Wheeler RJ, Tesarova M, Flegontov P, Jirsova D, et al. Extensive flagellar
566 remodeling during the complex life cycle of Paratrypanosoma, an early-branching trypanosomatid. Proc Natl
567 Acad Sci U S A. 2017;114(44):11757-62. Epub 20171016. doi: 10.1073/pnas.1712311114. PubMed PMID:
568 29078369; PubMed Central PMCID: PMCPMC5676924.

569 40. Rojas R, Segovia C, Trombert AN, Santander J, Manque P. The effect of tunicamycin on the glucose uptake,
570 growth, and cellular adhesion in the protozoan parasite *Crithidia fasciculata*. Current Microbiology.
571 2014;69(4):541-8. doi: 10.1007/s00284-014-0620-x.

572 41. Makin L, Gluenz E. cAMP signalling in trypanosomatids: role in pathogenesis and as a drug target. Trends in
573 parasitology. 2015;31(8):373-9. Epub 20150521. doi: 10.1016/j.pt.2015.04.014. PubMed PMID: 26004537;
574 PubMed Central PMCID: PMCPMC4534343.

575 42. Gonzales-Perdomo M, Romero P, Goldenberg S. Cyclic AMP and adenylate cyclase activators stimulate
576 *Trypanosoma cruzi* differentiation. Exp Parasitol. 1988;66(2):205-12. doi: 10.1016/0014-4894(88)90092-6.
577 PubMed PMID: 2840306.

578 43. Rolin S, Paindavoine P, Hanocq-Quertier J, Hanocq F, Claes Y, Le Ray D, et al. Transient adenylate cyclase
579 activation accompanies differentiation of *Trypanosoma brucei* from bloodstream to procyclic forms. Mol
580 Biochem Parasitol. 1993;61(1):115-25. doi: 10.1016/0166-6851(93)90164-s. PubMed PMID: 8259124.

581 44. Laxman S, Riechers A, Sadilek M, Schwede F, Beavo JA. Hydrolysis products of cAMP analogs cause
582 transformation of *Trypanosoma brucei* from slender to stumpy-like forms. Proceedings of the National Academy
583 of Sciences. 2006;103(50):19194-9. doi: 10.1073/pnas.0608971103.

584 45. Oberholzer M, Saada EA, Hill KL. Cyclic AMP regulates social behavior in African trypanosomes. mBio.
585 2015;6(3):e01954-14. Epub 20150428. doi: 10.1128/mBio.01954-14. PubMed PMID: 25922395; PubMed Central
586 PMCID: PMCPMC4436052.

587 46. Shaw S, Demarco SF, Rehmann R, Wenzler T, Florini F, Roditi I, et al. Flagellar cAMP signaling controls
588 trypanosome progression through host tissues. Nature Communications. 2019;10(1). doi: 10.1038/s41467-019-
589 08696-y.

590 47. Kelly FD, Sanchez MA, Landfear SM. Touching the surface: diverse roles for the flagellar membrane in
591 kinetoplastid parasites. Microbiol Mol Biol Rev. 2020;84(2). Epub 20200401. doi: 10.1128/MMBR.00079-19.
592 PubMed PMID: 32238446; PubMed Central PMCID: PMCPMC7117551.

593 48. Tyler KM, Fridberg A, Toriello KM, Olson CL, Cieslak JA, Hazlett TL, et al. Flagellar membrane localization
594 via association with lipid rafts. J Cell Sci. 2009;122(Pt 6):859-66. Epub 20090224. doi: 10.1242/jcs.037721.
595 PubMed PMID: 19240119; PubMed Central PMCID: PMCPMC2714428.

596 49. Bertiaux E, Mallet A, Fort C, Blisnick T, Bonnefoy S, Jung J, et al. Bidirectional intraflagellar transport is
597 restricted to two sets of microtubule doublets in the trypanosome flagellum. J Cell Biol. 2018;217(12):4284-97.
598 Epub 20181001. doi: 10.1083/jcb.201805030. PubMed PMID: 30275108; PubMed Central PMCID:
599 PMCPMC6279389.

600 50. Dean S, Sunter J, Wheeler RJ, Hodkinson I, Gluenz E, Gull K. A toolkit enabling efficient, scalable and
601 reproducible gene tagging in trypanosomatids. Open Biol. 2015;5(1):140197. doi: 10.1098/rsob.140197. PubMed
602 PMID: 25567099; PubMed Central PMCID: PMCPMC4313374.

603 51. Schumann Burkard G, Jutzi P, Roditi I. Genome-wide RNAi screens in bloodstream form trypanosomes
604 identify drug transporters. Mol Biochem Parasitol. 2011;175(1):91-4. Epub 20100922. doi:
605 10.1016/j.molbiopara.2010.09.002. PubMed PMID: 20851719.

606 52. Tetaud E, Lecuix I, Sheldrake T, Baltz T, Fairlamb AH. A new expression vector for *Crithidia fasciculata* and
607 *Leishmania*. Mol Biochem Parasitol. 2002;120(2):195-204. doi: 10.1016/s0166-6851(02)00002-6. PubMed
608 PMID: 11897125.

609 53. Blaazer AR, Singh AK, de Heuvel E, Edink E, Orrling KM, Veerman JJN, et al. Targeting a subpocket in
610 *Trypanosoma brucei* Phosphodiesterase B1 (TbrPDEB1) enables the structure-based discovery of selective
611 inhibitors with trypanocidal activity. J Med Chem. 2018;61(9):3870-88. Epub 20180501. doi:
612 10.1021/acs.jmedchem.7b01670. PubMed PMID: 29672041; PubMed Central PMCID: PMCPMC5949723.

613 54. de Heuvel E, Singh AK, Boronat P, Kooistra AJ, van der Meer T, Sadek P, et al. Alkynamide phthalazinones
614 as a new class of TbrPDEB1 inhibitors (Part 2). Bioorg Med Chem. 2019;27(18):4013-29. Epub 20190705. doi:
615 10.1016/j.bmc.2019.06.026. PubMed PMID: 31378593.

616 55. Salado IG, Singh AK, Moreno-Cinos C, Sakaine G, Siderius M, Van der Veken P, et al. Lead optimization of
617 phthalazinone phosphodiesterase inhibitors as novel antitrypanosomal compounds. J Med Chem.
618 2020;63(7):3485-507. Epub 20200326. doi: 10.1021/acs.jmedchem.9b00985. PubMed PMID: 32196340.

619

620

621 ## Figure Legends

622

623 **Figure 1.** An adherence assay reveals features of *C. fasciculata* attachment. **A)** Schematic showing steps of the
624 assay, including the variables tested. **B)** Representative images showing attached rosettes produced by varying the
625 initial plating time. The dashed red lines were drawn to indicate what was counted manually as individual
626 rosettes, clusters containing 4 or more cells. **C)** Quantitation of the experiment shown in B. This experiment was
627 performed in triplicate. Error bars show standard error. **D)** The effect of initial cell concentration on adherence.
628 10^7 cells/mL from cultures in different phase of growth, were adhered for each sample. Quantitation of a
629 representative experiment of three replicates is shown with median values indicated by red lines. **E)** Rosettes
630 resulting from adherence of different numbers of cells, all derived from a mid-log phase culture (10^7 cells/mL). A
631 representative experiment of three replicates is shown. Red lines indicate median values, and the blue dotted line
632 represents the proportion of plated cells that were able to adhere.

633

634 **Figure 2.** Flagellar shortening occurs at a relatively constant rate following an initial adhesion event. **A)**
635 Following 5 minutes of plating and subsequent washing, cells were observed at the indicated times and the length
636 of the flagellum was measured in 20 representative cells (different cells were measured at each time point). **B)** An
637 example of a single cell undergoing flagellar shortening. The numbers indicate time in minutes. The schematic on
638 the right shows a representation of the length of the flagellum at the beginning (red) and end (blue) of the time
639 course.

640

641 **Figure 3.** Transmission electron microscopy reveals structural differences between attached and swimming cells.
642 **A)** Cross section through *C. fasciculata* parasites adhered to tissue culture plastic (Fig S2, yellow plane).
643 Asterisks indicate hemidesmosomes at the distal tip of the shortened flagella. Scale bar is 1 µm. The dotted box
644 indicates the region enlarged in panel A'. **A')** Close up of a hemidesmosome (hd) from one of the cells in panel A.
645 Desmosome-like FAZ structures, connecting the flagellum to the cell body, are also observed (fz). Scale bar is
646 200 nm. **B)** and **C)** Additional examples of hemidesmosomes (hd) and desmosome-like FAZ (fz). The cell in C)
647 was scraped from the dish prior to fixation. Scale bar is 200 nm. **D)** Sectioning *en face* shows a region near the
648 end of the flagellum in an adherent cell (Fig S2, blue planes). The flagellar membrane is enlarged and no flagellar
649 axoneme can be observed. Instead, diffuse filaments probably comprising the hemidesmosome are seen. Scale bar
650 is 200 nm. **E)** Another example of a hemidesmosome sectioned *en face*. Scale bar is 200 nm. **F)** Section of a
651 swimming cell shows the flagellum extending from the flagellar pocket. Dotted box indicates the region enlarged
652 in F'. Scale bar is 1 µm. **F')** Higher magnification view of the flagellar pocket of a swimming cell. FAZ structures
653 link the flagellar membrane to the flagellar pocket membrane, but no hemidesmosome is seen. The slight bulge in
654 the flagellum where it exits the pocket may be a physical correlate to the site of initial adhesion. Filamentous
655 material can be observed in the flagellar pocket of the swimming cell but was never observed on the surface. In
656 contrast, the surface of attached cells, **G)** was covered with this material. Some of the same material is also visible
657 in panels A, B, C, D, and E. Scale bar F' and G is 400 nm.

658

659 **Figure 4.** Phosphodiesterase inhibitors block *C. fasciculata* adherence. **A)** Adherence assays performed in the
660 presence of 10 µM of either NPD-001 (NPD1) or NPD-008 (NPD8). The number of single adhered cells at 2
661 hours (open circles) and the number of rosettes (≥ 4 cells, gray squares) at 24 hours were counted and compared
662 to those from a vehicle-treated control sample (Veh) and an untreated sample (Con). Treatments were present in
663 the media both during the 2-hour plating time and the subsequent 24 hours of culture. All comparisons were
664 made. Asterisks indicate Kruskal-Wallis test with Dunn's correction $P<0.0001$ (****) and $P<0.05$ (*) **B)**
665 Adhesion assays comparing vehicle and untreated controls to assays performed in the presence of different
666 concentrations of NPD-001 or **C**) NPD-226. The number of single adhered cells at 2 hours (open circles) and the
667 number of rosettes (≥ 4 cells, gray squares) at 24 hours were counted. All comparisons were made, but only the

668 groups that are significantly different from the adjacent treatment are shown. Asterisks indicate Kruskal-Wallis
669 test with Dunn's correction P<0.0001 (****), and P<0.01 (**).

670

671 **Figure 5.** NPD-001 does not affect the growth rate of *C. fasciculata*. **A)** Graph of *C. fasciculata* growth in
672 shaking cultures assayed over approximately 31 h in standard medium (Control; blue circles), medium
673 supplemented containing 10 µM NPD-001 in vehicle (NPD1; orange diamonds), or medium containing vehicle
674 only (Vehicle, red squares). **B)** Time encoded movies were used to measure the doubling time of established
675 attached cultures after the addition of NPD-001 in vehicle, or in vehicle alone. The red line indicates the mean. No
676 significant difference was noted between the doubling times.

677

678 **Figure 6.** Components of cAMP signaling localize to different domains of the flagellum in *C. fasciculata*
679 swimmers. Deconvolved confocal images of GFP and YFP fusion proteins and DAPI staining of nuclear and
680 kDNA of fixed swimmer and attached cell cultures. A Z-stack of the entire cells and rosettes were captured.
681 Fluorescent images are shown individually and merged. A brightfield image for each is included for reference and
682 was used to generate the red dashed outline of the flagellum in the merged and brightfield images. An overlay of
683 fluorescent channels on the corresponding brightfield image also shows the extent of GFP or YFP signal with
684 respect to the length of the flagellum (Fig S4). The scale bars are 5 µm. Western blots of extracts of swimmers
685 (Sw) and attached (Ad) cells of each line are included supporting the presence of the correct size GFP- or YFP-
686 fusion protein (Fig S3) in both swimmer and attached cells regardless of their localization patterns. Equivalent
687 loading was confirmed by re-probing blots with an anti-BiP antibody. Parental Cf-C1 cells lack GFP signal in
688 swimmers and adherent cells as well as by western analysis (Fig S5).

689

690 **Figure 7.** Model of the developmental transition from swimmer to adherent cell. The localizations of *Cf*RAC1
691 (red), and *Cf*PDEA (blue) are indicated. Minutes following adhesion via the region of the flagellum near the cell

692 body (orange), the process of flagellar shortening begins. Flagellar shortening brings *Cf*RAC1 closer to the cell
693 body. Eventually the source of cAMP is close enough to the cell and the sink for cAMP (*Cf*PDEA) is reduced
694 such that cAMP levels rise above a critical threshold in the cell body (shown on the graph by a star). This
695 promotes differentiation to the adherent cell fate characterized cytoplasmic localization of *Cf*RAC1 and *Cf*PDEA
696 by robust changes in gene regulation and formation of a hemidesmosome.

697

698 **Figure S1.** Density dependent changes to *C. fasciculata* morphology. **A)** Giemsa-stained samples of cells at log-
699 phase (10^7 cells/mL) or past log-phase growth (10^8 cells/mL). Scale bar is 10 µm. **B)** Plot of individual measured
700 cell lengths in micrometers. Cells were measured along the anterior-posterior axis of the cell body excluding the
701 flagellum. The data are normally distributed (Shapiro-Wilk test). The red line indicates the mean and standard
702 deviation. An unpaired t test indicates the cell length distributions are significantly different with a P value of
703 0.005.

704

705 **Figure S2.** Illustration of sectioning planes used for transmission electron microscopy. An adherent cell shown in
706 cross section (yellow plane; sections in Fig 3A-C, and F-G). Sections cut *en face* at different distances from the
707 culture plate (blue planes). Depending on the position of the *en face* section relative to the culture plate, the
708 osmiophilic hemidesmosome-like structure will appear darker (Fig 3E) or lighter (Fig 3D) and other cell features,
709 such as the cell cytoplasm and mitochondrion may be visible (Fig 3D).

710

711 **Figure S3.** Phosphodiesterase inhibitor NPD-055 partially reduces *C. fasciculata* adherence. Adherence assays
712 performed in the presence in the presence of different amounts of NPD-055 compared to vehicle-only treated
713 controls. The number of single adhered cells at 2 hours (open circles) and the number of rosettes (≥ 4 cells, gray
714 squares) at 24 hours were counted and compared to those from a vehicle-treated control sample (Veh). Treatments
715 were present in the media both during the 2-hour plating time and the subsequent 24 hours of culture. Data are not

716 normally distributed. Red lines indicate the median. All comparisons were made, but only the groups that are
717 significantly different from the adjacent treatment are shown. Asterisks indicate Kruskal-Wallis test with Dunn's
718 correction P<0.0001 (****), P<0.001 (***), and P<0.05 (*).

719

720 **Figure S4.** Schematic diagram of tagged proteins used for localization studies. Open reading frames encoding
721 *Cf*PDEA (CFAC1_140020300) and *Cf*RAC1 (CFAC1_090006500) were cloned without their C-terminal stop
722 codon into a vector resulting in an in-frame fusion with the coding sequence of GFP (green rectangle). The
723 resulting constructs were transfected into *C. fasciculata* and lines episomally expressing the tagged proteins were
724 selected using hygromycin. A single allele of *Cf*PF16 (CFAC1_170028000) was fused in-frame at its C-terminus
725 with YFP (yellow rectangle) by homologous recombination followed by neomycin selection. The number of
726 amino acids (aa) for each fusion protein is provided. Domains and their relative positions indicated in the different
727 constructs are 3'5'-cyclic nucleotide phosphodiesterase, catalytic domain (PDEase; IPR002073), Periplasmic
728 binding protein-like I (PBPL; IPR028082), Nucleotide cyclase (AC; IPR029787), Armadillo-type fold
729 (Armadillo-fold; IPR016024), signal peptide for secretion (SP), and transmembrane domain (TM). Further details
730 are provided in the Materials and Methods.

731

732 **Figure S5.** Overlay images show the extent of fluorescent signal along the swimming cell flagellum. Overlay of
733 the brightfield and fluorescent images of parental Cf-C1, *Cf*PDEA::GFP, *Cf*RAC1::GFP, and *Cf*PF16::YFP from
734 Figure 6. The fluorescence of *Cf*PDEA::GFP reaches the cell body and weakly inside, similar, but less uniform as
735 *Cf*PF16::YFP. In contrast, *Cf*RAC1::GFP is more restricted to the distal part of the flagellum. Parental cells lack
736 GFP signal. The scale bars are 5 μm.

737

738 **Figure S6.** Parental Cf-C1 lack GFP signal by confocal and western blot analyses. Deconvolved confocal images
739 of GFP and DAPI images of fixed swimmer and attached cell cultures taken with the same settings as shown in

740 Figure 6. Fluorescent images are shown individually and merged. A brightfield image for each is included for
741 reference and was used to generate the dashed outline of the flagellum in the merged image. A western blot of
742 extracts of swimming and attached cells probed with anti-GFP and anti-BiP (loading control) antibodies.

743

744 **Video S1.** $4x10^5$ parental Cf-C1 cells were added to wells of a 24-well plate and imaged at 75 second intervals for
745 16 hours to obtain movies of *C. fasciculata* as they adhere. This video shows the full imaging frame at 60x
746 magnification, which highlights several adhesion events occurring during the imaging time. Note an oblong out-
747 of-focus object appears to the left of center. The scale bar is 50 µm.

748

749 **Video S2.** Close up and cropped version of Video S1. For reference, the same oblong out-of-focus object that is
750 visible near the center of Video S1 appears at the left edge of this video. Note when a dividing pair of cells first
751 adheres to the culture dish surface (time 5:42:30), one cell swims away. The other remains characteristically
752 attached at the junction between the cell body and the flagellum. Both the cell body and the flagellum move
753 independently until the flagellum is retracted and the cell body is round (time 8:40:00). The first division as an
754 adherent cell occurs at approximately 9:08:45. One of the adherent daughters divides again approximately 4 hours
755 and 4 minutes later (time 13:12:30). The other adherent daughter divides approximately 5 hours and 25 minutes
756 later (time 14:33:45). The scale bar is 10 µm.

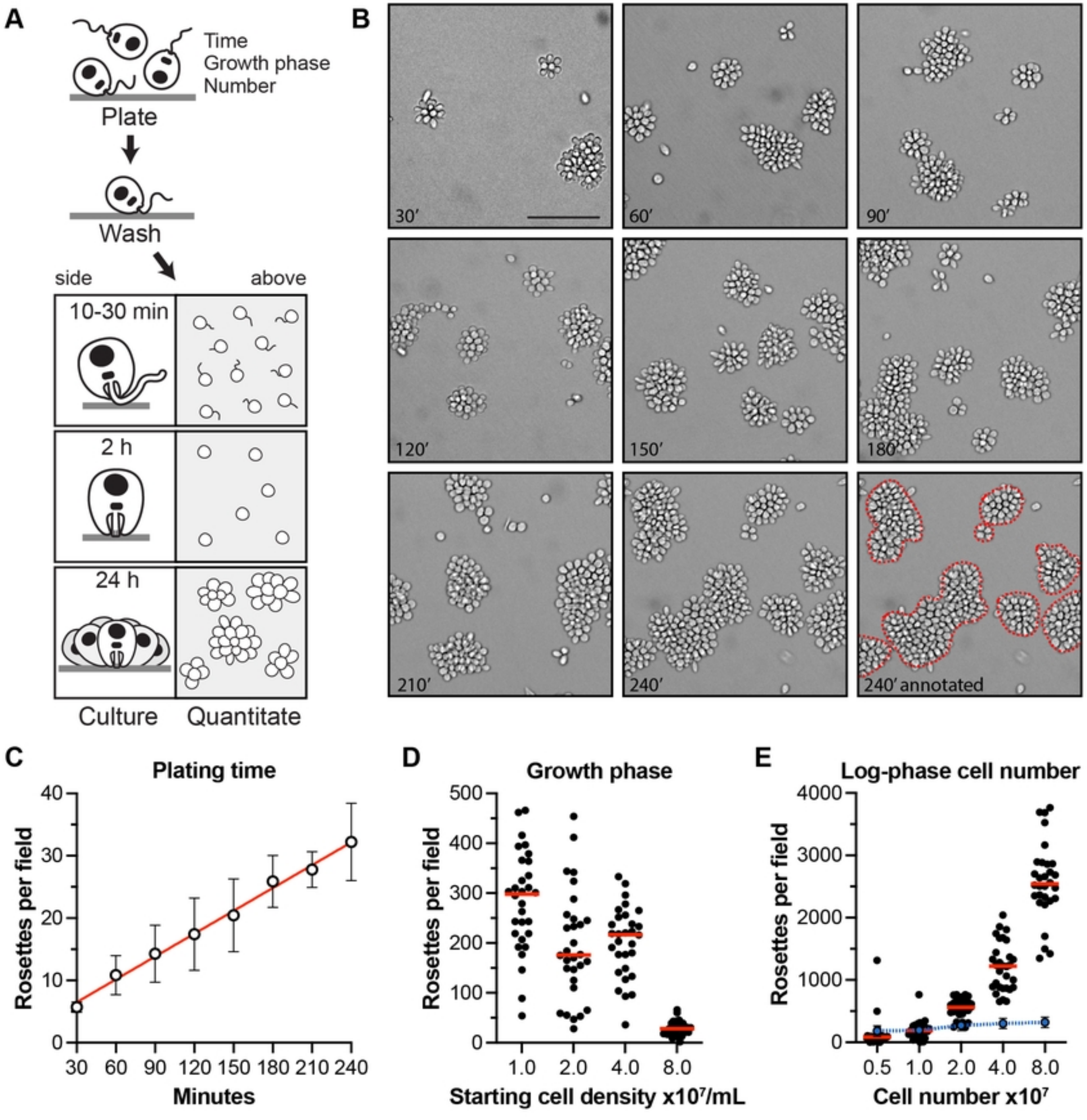
A
Time
Growth phase
Number
Plate
Wash
side
above
10-30 min
2 h
24 h
Culture
Quantitate
B
30′
60′
90′
120′
150′
180′
210′
240′
240′ annotated
C
Plating time
Rosettes per field
Minutes
D
Growth phase
Rosettes per field
Starting cell density x10⁷/mL
E
Log-phase cell number
Rosettes per field
Cell number x10⁷

Figure 1

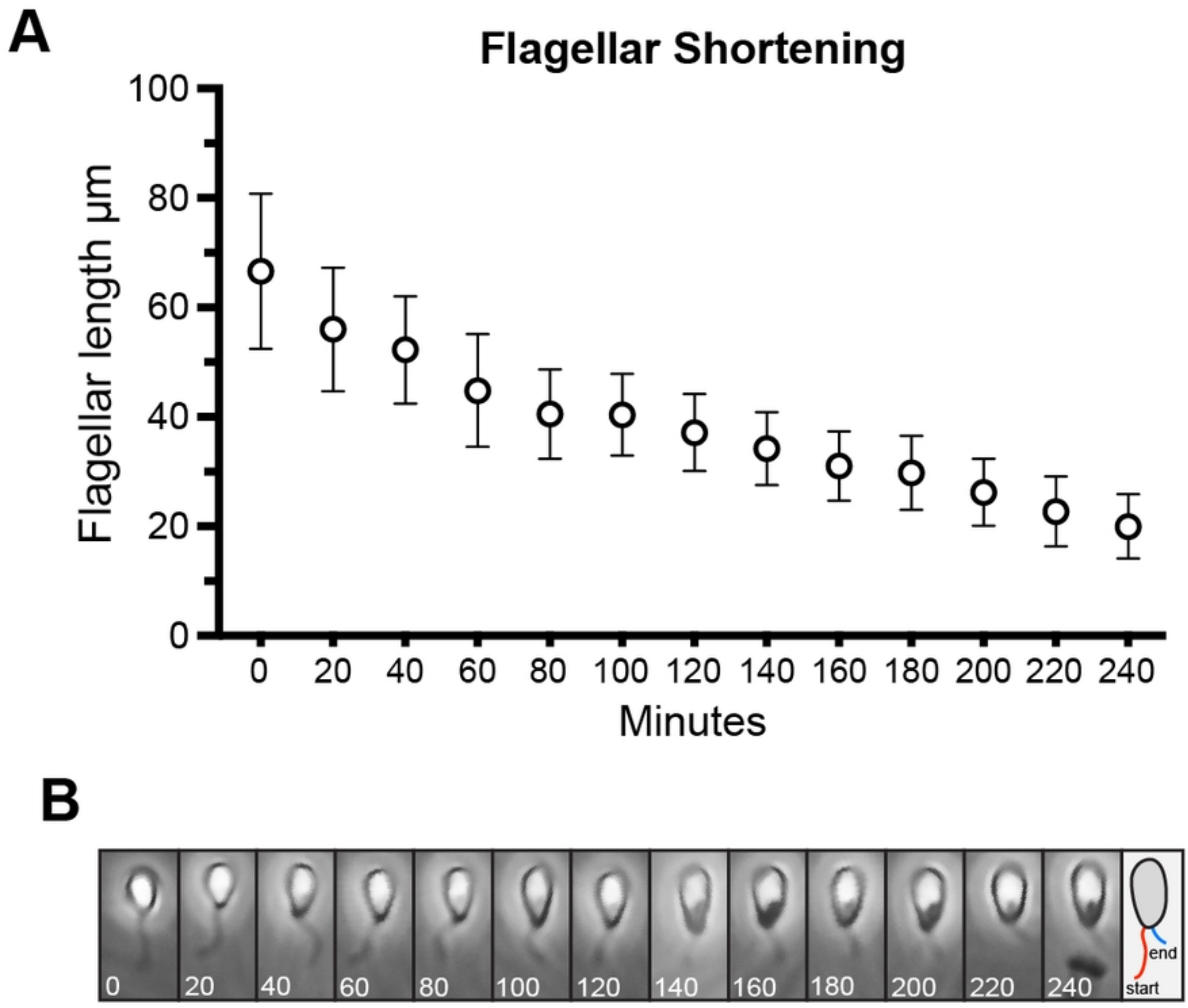
A
Flagellar Shortening
Flagellar length µm
100
80
60
40
20
0
0
20
40
60
80
100
120
140
160
180
200
220
240
Minutes
B
0
20
40
60
80
100
120
140
160
180
200
220
240
end
start

Figure 2

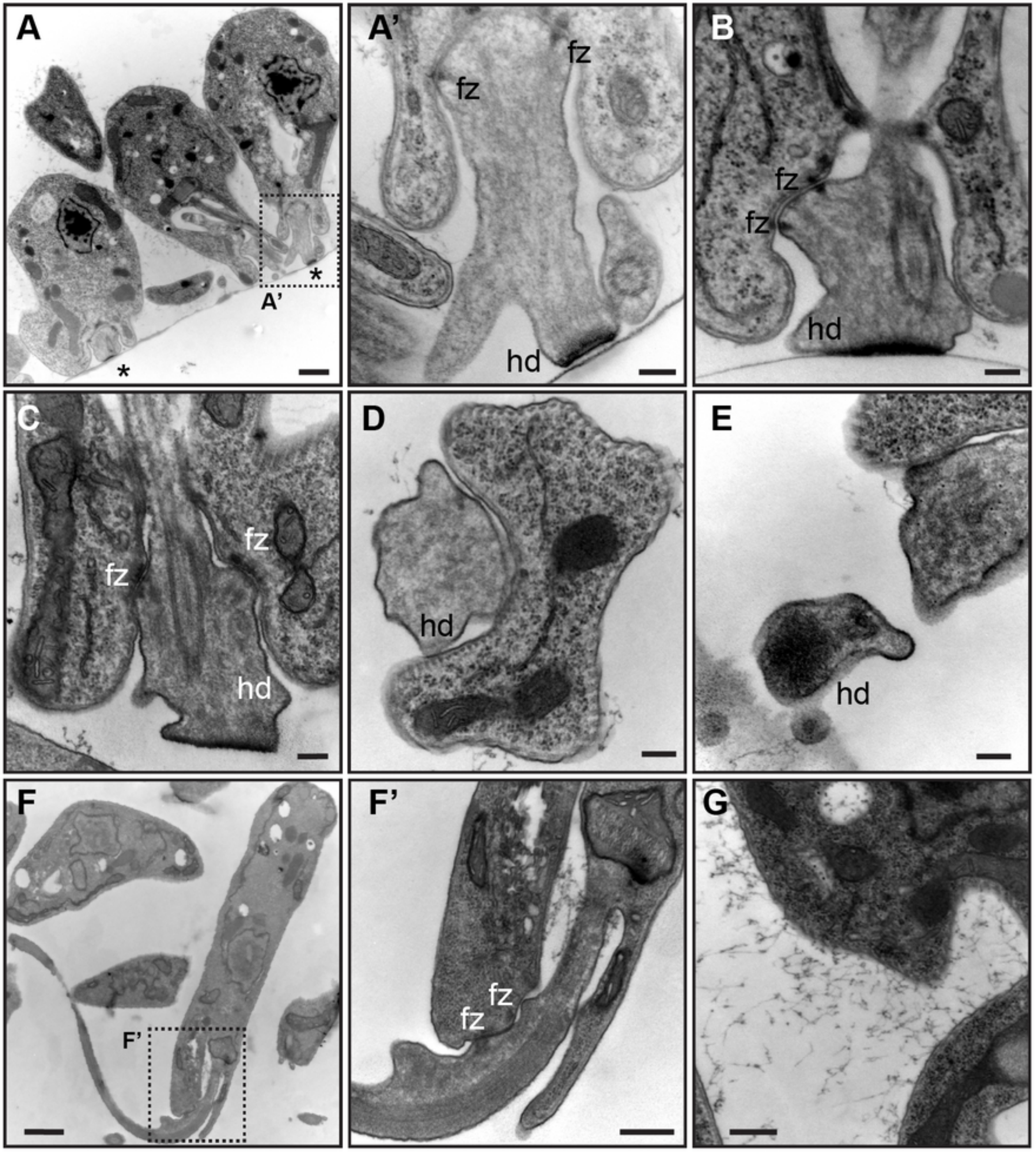

Figure 3

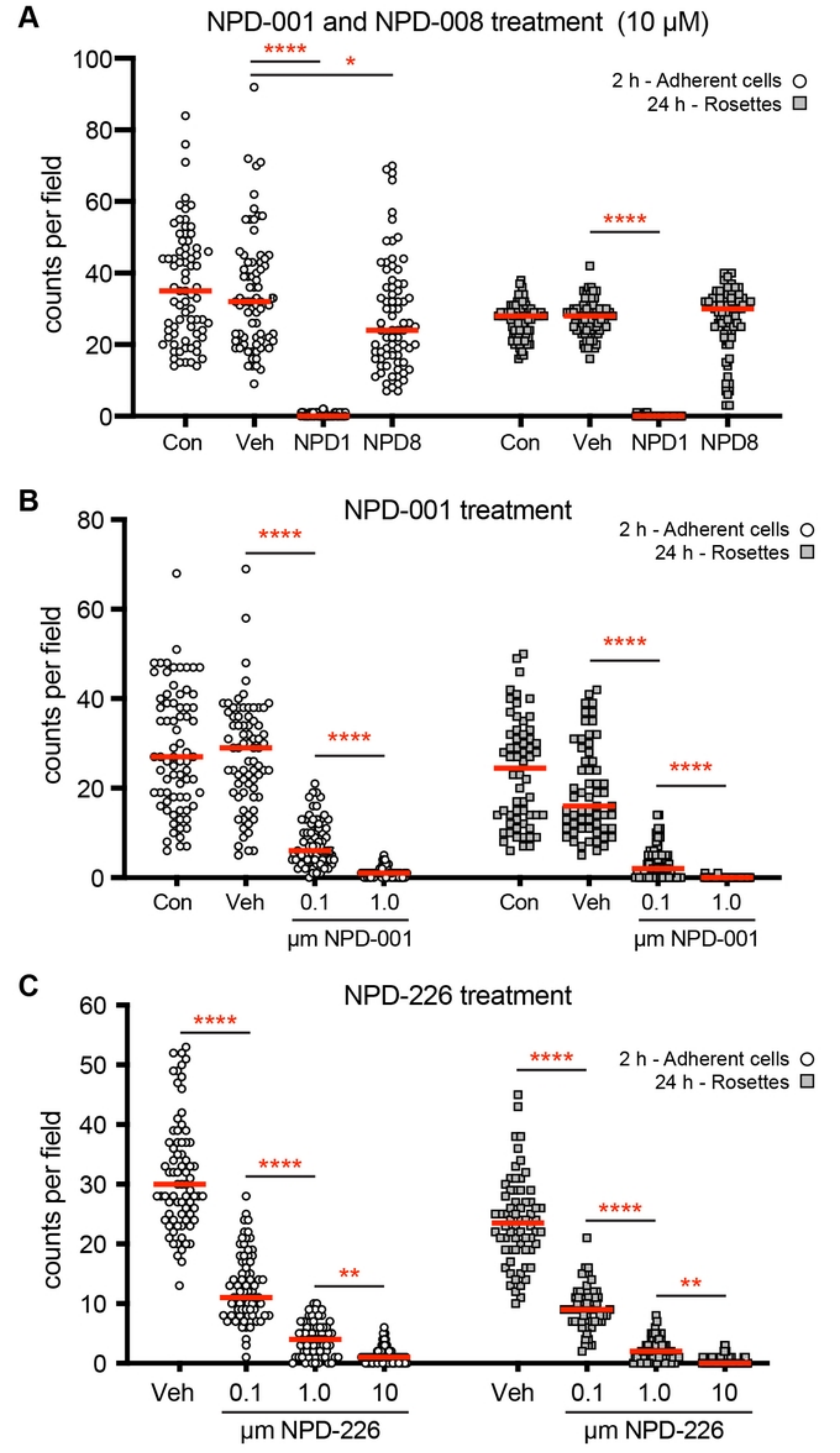
A
NPD-001 and NPD-008 treatment (10 μM)
counts per field
2 h - Adherent cells
24 h - Rosettes
Con
Veh
NPD1
NPD8
B
NPD-001 treatment
0.1
1.0
μm NPD-001
C
NPD-226 treatment
10
μm NPD-226

Figure 4

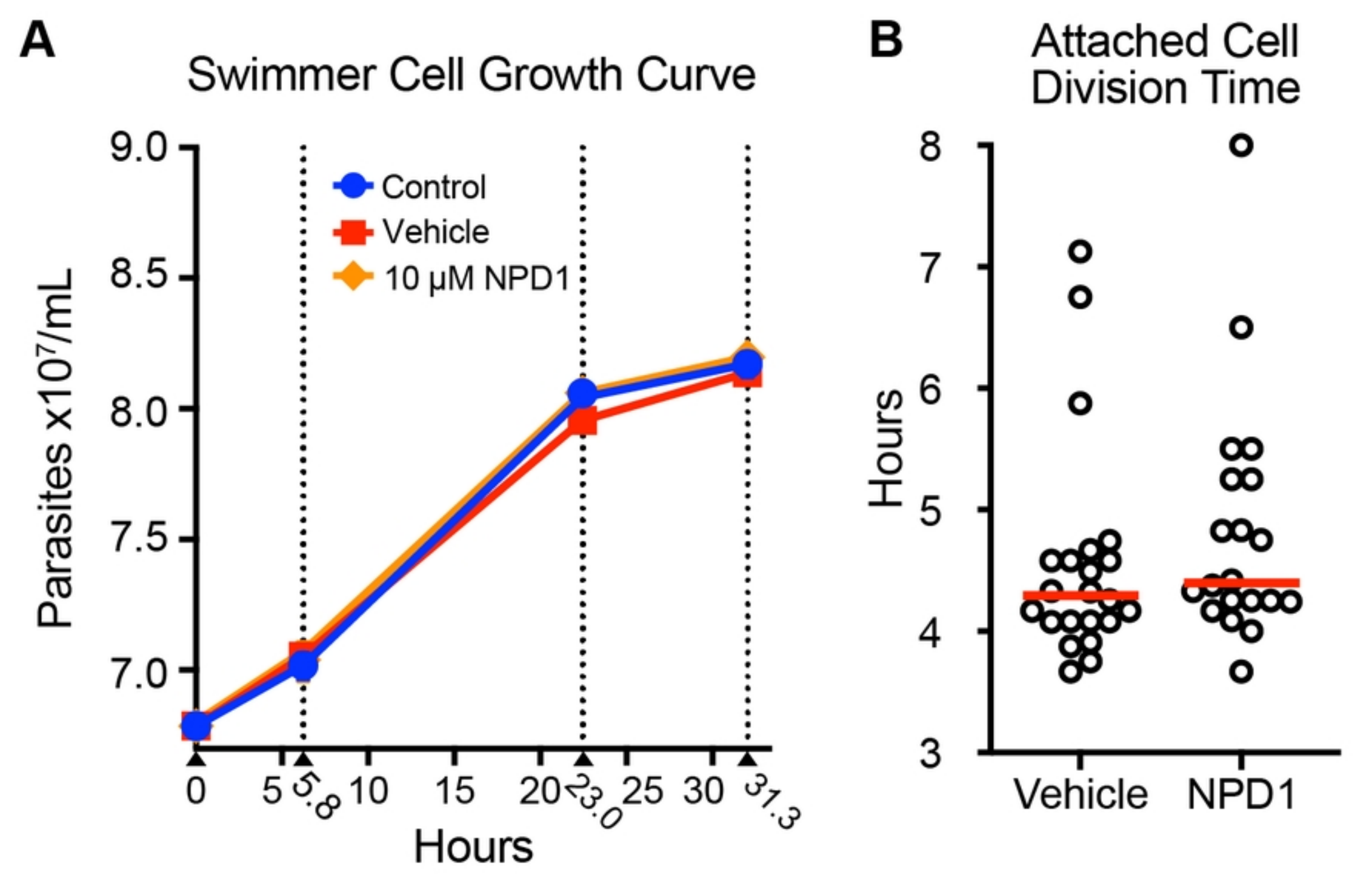
A
Swimmer Cell Growth Curve
Control
Vehicle
10 μM NPD1
Parasites x10^7/mL
9.0
8.5
8.0
7.5
7.0
0
5
5.8
10
15
20
23.0
25
30
31.3
Hours
B
Attached Cell Division Time
Hours
8
7
6
5
4
3
Vehicle
NPD1

Figure 5

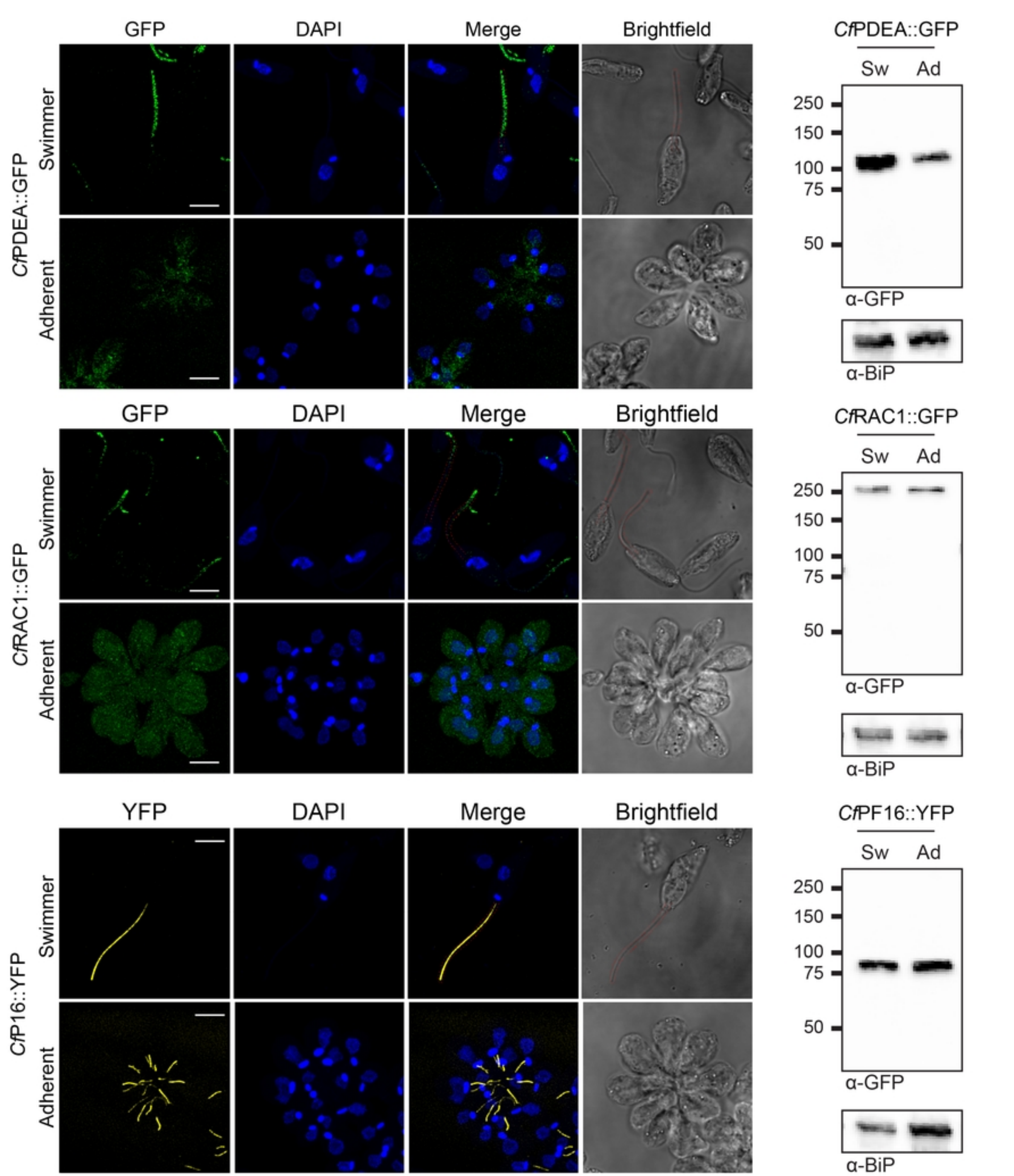
GFP
DAPI
Merge
Brightfield
CfPDEA::GFP
Swimmer
Adherent
CfPDEA::GFP
Sw
Ad
250
150
100
75
50
α-GFP
α-BiP
GFP
DAPI
Merge
Brightfield
CfRAC1::GFP
Swimmer
Adherent
CfRAC1::GFP
Sw
Ad
250
150
100
75
50
α-GFP
α-BiP
YFP
DAPI
Merge
Brightfield
CfP16::YFP
Swimmer
Adherent
CfP16::YFP
Sw
Ad
250
150
100
75
50
α-GFP
α-BiP

Figure 6

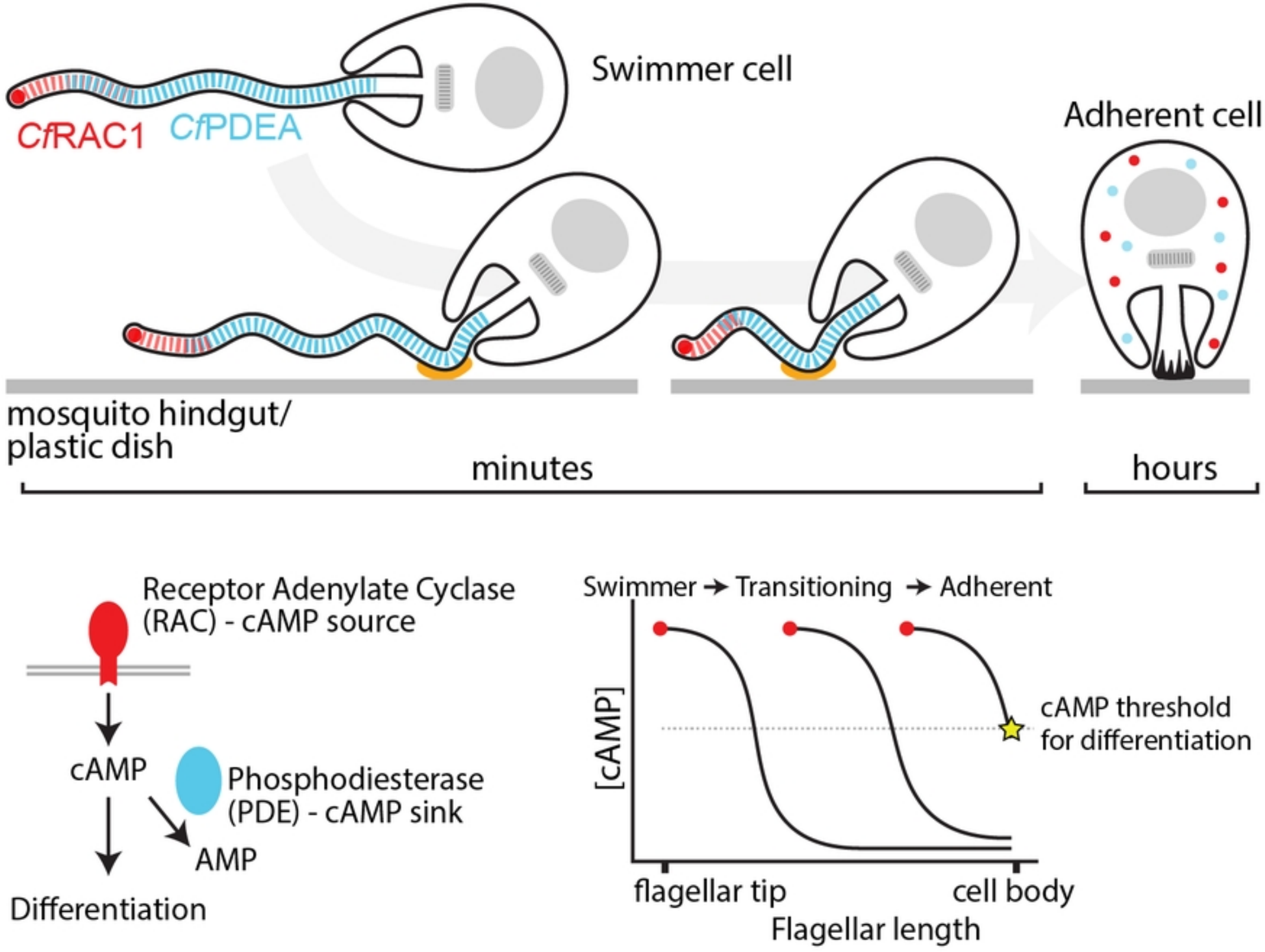
Swimmer cell
CfRAC1
CfPDEA
Adherent cell
mosquito hindgut/
plastic dish
minutes
hours
Receptor Adenylate Cyclase
(RAC) - cAMP source
cAMP
Phosphodiesterase
(PDE) - cAMP sink
AMP
Differentiation
Swimmer → Transitioning → Adherent
[cAMP]
cAMP threshold
for differentiation
flagellar tip
cell body
Flagellar length

Figure 7